

# Efficient Coupled Time Integration Methods for Transonic Aeroelastic Analysis

M. G. Chae\*, S. H. Park\*, J.Y. Lee\*\* and J. S. Bae\*\*  
Corresponding author: pish@konkuk.ac.kr

\* Department of Aerospace Information Engineering,  
Konkuk University, Seoul, South Korea

\*\* Department of Aerospace and Mechanical Engineering,  
Korea Aerospace University, Goyang-si, South Korea

**Abstract:** The coupled time integration methods(CTIM) based on computational structural dynamics(CSD) and computational fluid dynamics(CFD) have been developed to predict the aeroelastic phenomena such as flutter or buffet in transonic or low supersonic regimes. Staggered algorithms are basically applied for data transfer when CFD using implicit temporal scheme and CSD using explicit temporal scheme are loosely coupled. An iterative staggered algorithm was proposed that repeatedly converges structural equations while solving the CFD sub-iteration to overcome the limitations of the conventional staggered algorithm. For comparison with other temporal schemes, the convergence test with the time step was conducted. The flutter-boundary prediction of the AGARD 445.6 wing is used to verify the developed code and demonstrate the accuracy and efficiency.

*Keywords:* CFD-CAE Coupling, Coupled Time Integration Method, Time Lagging, Staggered Algorithm

## 1 Introduction

Flutter is the self-excited structural oscillation due to the interaction between the inertial, elastic and aerodynamic forces. Modern aircraft are designed to have high flexibility inevitably to have more and more lightweight. In addition, the nonlinearity that is related to the viscous effect, turbulence and shock waves on the airfoil causes the flutter dip which is a phenomenon where flutter boundary is drastically lowered. Therefore, the aeroelastic stability analysis in the transonic region is indispensable for the conceptual design stage of modern aircraft. Computational studies on aeroelastic analysis have been continuously conducted [1-6].

Coupling methods for fluid-structure integration can be classified into monolithic approach and partitioned approach. A monolithic approach computes the reconstructed fluid-structure integrated equation [7,8], which can improve the time accuracy. However, in case of the complicated aeroelastic analysis, it is not easy to formulate the integration between fluid and structural dynamic equations. A partitioned approach, called by staggered algorithm, sequentially integrates unsteady equations by transferring each solution as an initial condition. It is simple and efficient to develop because it uses existing structure and fluid analysis techniques. Conventional staggered algorithms, however, have the first-order temporal accuracy with respect to the aerodynamic forces used in time advance of the structural dynamic equations. This temporal error, called the time lagging, can be reduced by using a

more smaller time step, but the computation time increases.

To overcome the time lagging, Alonso and Jameson [9] used a tightly coupled method with an explicit method for diagonalized state space equation. At time level  $n$ , the pseudo-time calculation is conducted, and the flow information is sent to the structural solver. Then the new deformation is transferred to the flow solver. It is tried to eliminate the time lagging by exchanging the aerodynamic forces and structural deformation repeatedly in every pseudo time step. For this method, at least 100 pseudo-time steps are generally needed for the explicit schemes to ensure adequate convergence [10].

Farhat and Lesoinne [11] proposed improved serial/parallel method. The improved serial staggered algorithm based on midpoints rule predicts the position of the  $n+1/2$  step using the structural position and velocity at the  $n$  step, and transferred them to the flow solver to obtain the aerodynamic forces at the  $n+1/2$  step. The parallel staggered algorithm forces to advance the structure integration twice in one time step, as a prediction and correction step. This strategy helps overcome the time lagging by exchanging aerodynamic and structure information at  $n+1/2$  step.

In this study, an aeroelastic analysis solver is developed by combining structural dynamic equations with modal approach and in-house CFD code that is based on structure grid system. Partitioned approach requires aerodynamic forces mapping and structural displacement interpolation. Because the number of grid points in the moving boundary is generally very large, The spline method and the inverse transform mapping method using the equilibrium of virtual work [12, 13] are very large interpolation matrix operations. The spline interpolation matrix is parallelized based on the moving boundary of CFD. It is important to maintain the temporal accuracy related to aerodynamic forces for staggered algorithm. The iterative method can provide converged solutions of both structure solver and flow solver at the next time step through repetitive coupling of the fluid-structure. The dual time stepping method based on the diagonalized alternating directional implicit (DADI) is applied to the unsteady time-accurate CFD simulation. The 4<sup>th</sup> order Runge-Kutta method is applied as the structural time integration method. Time step convergence study for the AGARD 445.6 wing tested on transonic dynamics tunnel(TDT) [14] was conducted to compare the coupled time integration methods.

## 2 Numerical Approach

### 2.1 Governing Equations in Flow Solver

The 3-dimensional compressible Navier-Stokes equations [15] can be written as:

$$\frac{\partial \mathbf{Q}}{\partial t} + \frac{\partial (\mathbf{F}_j - \mathbf{F}_{vj})}{\partial x_j} = 0 \quad j=1,2,3 \quad (1)$$

where  $\mathbf{Q}$  is the conservative variable vectors,  $\mathbf{F}_j$  and  $\mathbf{F}_{vj}$  are the inviscid and viscous flux vectors in each direction, respectively:

$$\mathbf{Q} = \begin{bmatrix} \rho \\ \rho u_i \\ \rho E \end{bmatrix}, \quad \mathbf{F}_i = \begin{bmatrix} \rho u_j \\ \rho u_j u_i + p \delta_{ij} \\ \rho u_j H \end{bmatrix}, \quad \mathbf{F}_{vj} = \begin{bmatrix} 0 \\ \sigma_{ij} + \sigma_{ij}^* \\ u_j (\sigma_{ij} + \sigma_{ij}^*) - q_j \end{bmatrix} \quad (2)$$

Here,  $\rho$ ,  $p$ ,  $E$  and  $H$  are the density, pressure, total energy and total enthalpy.  $u_j$  is the cartesian velocity components in each direction,  $\sigma$  and  $\sigma^*$  is the laminar and turbulent shear stress tensor, respectively and  $q_j$  is the heat fluxes in each direction. These components can be represented as follows:

$$\sigma_{ij} = \frac{\mu}{Re} \left( 2S_{ij} - \frac{2}{3} \delta_{ij} S_{kk} \right)$$

$$\sigma_{ij}^* = \frac{1}{Re} \left[ \mu_T \left( S_{ij} - \frac{2}{3} \delta_{ij} S_{kk} \right) - \frac{2}{3} (pk) \delta_{ij} \right]$$

$$q_j = -k \frac{\partial T}{\partial x_j} = -\mu \frac{C_p}{Pr} \frac{\partial T}{\partial x_j} = -\frac{\gamma \mu}{(\gamma - 1) Re Pr} \frac{\partial}{\partial x_j} \left( \frac{p}{\rho} \right)$$

The strain-rate tensor is given by

$$S_{ij} = \left( \frac{\partial u_i}{\partial x_j} + \frac{\partial u_j}{\partial x_i} \right)$$

The molecular viscosity is determined by the Sutherland law and the eddy viscosity,  $\mu_T$ , is evaluated using Spalarat-Allmaras(S-A) RANS turbulence model to determine the turbulent stresses in this paper.

## 2.2 Time Marching Scheme in Flow Solver

For unsteady flow solver, dual time stepping which is suggested by Jameson [16] is used to ensure the temporal accuracy in physical time step. The pseudo temporal term is added to unsteady residual including physical time step with high order differencing as follows:

$$\frac{\partial Q_{ijk}^{m+1}}{\partial \tau} + R_{ijk}^U = 0 \quad (3)$$

$$R_{ijk}^U = \frac{3Q_{ijk}^{n+1} - 4Q_{ijk}^n + Q_{ijk}^{n-1}}{2\Delta t} + R_{ijk}^{n+1} \quad (4)$$

The governing equations can be formulated by implicit form applying pseudo time step  $\Delta \tau$ .

$$\left[ \left( \frac{1}{J\Delta \tau} + \frac{3}{2J\Delta t} \right) I + \frac{\partial R}{\partial Q} \right] \Delta Q = -R_{ijk}^U (Q^m) \quad (5)$$

The Jacobian matrix of unsteady residual in governing equation is defined by spatial discretization scheme. The diagonalized alternating direction implicit(DADI) temporal scheme, which constructs an implicit operator by diagonalizing the matrix through approximate-factorization [17], is used to advance the solution in physical time.

## 2.3 Aeroelastic Equation of Motion

The aeroelastic equation of motion can be formulated by Hamilton Theorem for elastic models and is written in matrix form as follows [18].

$$[M_g] \{\ddot{q}(t)\} + [C_g] \{\dot{q}(t)\} + [K_g] \{q(t)\} = \{F(t)\} \quad (6)$$

where  $\{q(t)\}$  is the generalized displacement vector and  $[M_g]$ ,  $[C_g]$  and  $[K_g]$  is the generalized mass, damping and stiffness matrices respectively.  $\{Q(t)\}$  is the generalized aerodynamic forces as follows:

$$Q_i(t) = \frac{1}{2} \rho U^2 c_r^2 \int_{S^*} h_i(x^*, y^*) \Delta C_p(x^*, y^*, t) dS^* \quad (7)$$

where subscript  $i$  indicates the influence mode shapes and  $S^*$  is the non-dimensional area on the wing surface.  $0.5\rho U^2$  and  $C_r^2$  are the dynamic pressure and dimensional area associated with the root chord length which is the multiplied to make the dimensional forces.  $t$  represents physical time that is transformed from the non-dimensional time of the CFD. Eq. (4) can be reduced to the state vector forms as follows:

$$\{\dot{x}\} = [A] \{x(t)\} + [B] \{u(t)\} \quad (8)$$

where

$$[A] = \begin{bmatrix} [0] & [I] \\ -[M_g]^{-1}[K_g] & -[M_g]^{-1}[C_g] \end{bmatrix} \quad (9)$$

$$\{x(t)\} = \begin{Bmatrix} q(t) \\ \dot{q}(t) \end{Bmatrix}, \quad \{u(t)\} = \begin{Bmatrix} \{0\} \\ \{Q(t)\} \end{Bmatrix} \quad (10)$$

## 2.4 Time Marching scheme in Structural Solver

To solve the structural equations coupled with flow solver, a loosely coupled manner is used and can be seen as a conventional serial staggered procedure (CS) in figure 1, where  $x$  denotes the structure state vector  $[q, \dot{q}]^T$ ,  $U$  denotes the aerodynamic forces,  $u$  denotes the generalized aerodynamic forces with mode-shape vectors.

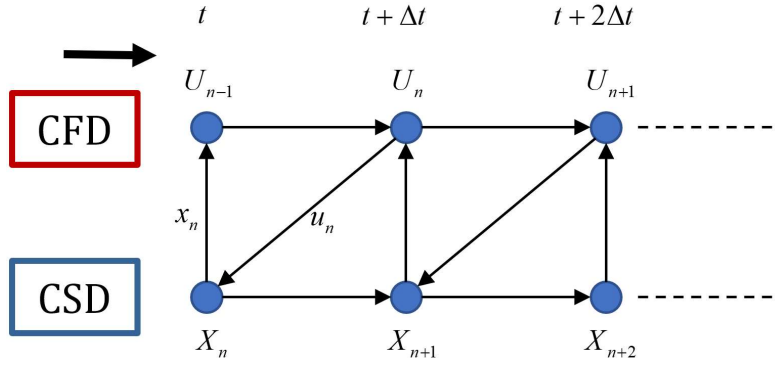


Figure 1: Schematic diagram of Conventional serial staggered algorithm.

In this method, the aerodynamic forces converged at each physical time step are transferred to the structural solver to obtain the generalized displacement, it is possible to facilitate the development by simply combining each independent solver. The structural differential equation (8) can be solved explicitly by Runge-Kutta method as follows:

$$\{x_{n+1}\} = \{x_n\} + (k_1 + 2k_2 + 2k_3 + k_4) / 6 \quad (11)$$

where

$$\begin{aligned} k_1 &= \Delta t ([A]\{x_n\} + [B]\{u_n\}) \\ k_2 &= \Delta t ([A]\{x_n + k_1/2\} + [B]\{u_{n+1/2}\}) \\ k_3 &= \Delta t ([A]\{x_n + k_2/2\} + [B]\{u_{n+1/2}\}) \\ k_4 &= \Delta t ([A]\{x_n + k_3\} + [B]\{u_{n+1}\}) \end{aligned} \quad (12)$$

The aerodynamic forces  $u_{n+1/2}$  and  $u_{n+1}$  except  $u_n$  are unknowns in Eq. (12). If these unknowns are replaced by  $u_n$ , Eq. (11) becomes conventional serial staggered algorithm and has the disadvantage that it is only first-order time-accurate, even when the underlying flow and structural solvers are of second-order time-accurate [11].

There are three methods for Eq. (11) to have higher order accuracy for aerodynamic forces. The first method (IS1, Improved Staggered algorithm 1) estimates the aerodynamic forces  $\{u_{n+1/2}\}$  and  $\{u_{n+1}\}$  by linear extrapolation using flow solution obtained at the previous step [19].

$$\begin{aligned} \{u_{n+1/2}\} &= \frac{15\{u_n\} - 10\{u_{n-1}\} + 3\{u_{n-2}\}}{8} \\ \{u_{n+1}\} &= 3\{u_n\} - 3\{u_{n-1}\} + \{u_{n-2}\} \end{aligned} \quad (13)$$

Substituting Eq. (13) into Eq. (12), Runge-Kutta solution in Eq. (11) provides a second-order time accuracy and the time step can be increased moderately, which can improve the efficiency of the computation. Furthermore, it is attractive that the computation time is nearly the same as the CS method because the computing time for the extrapolation is very small.

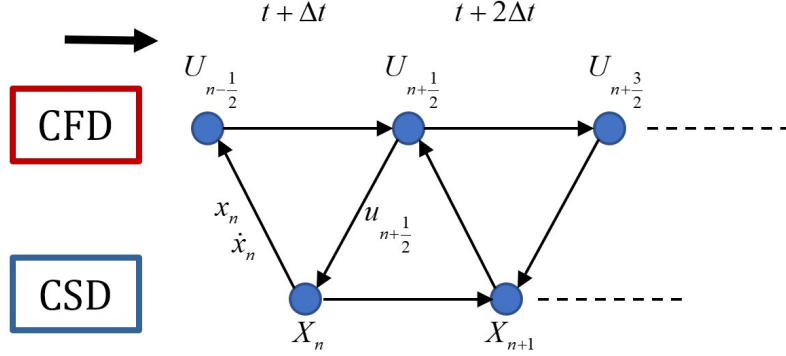


Figure 2: Schematic diagram of Improved serial staggered algorithm (IS2).

The second method (IS2, Improved Staggered algorithm 2) is to predict the aerodynamic forces on  $n + 1/2$  step by transferring the position on the next extrapolated  $n + 1/2$  step to the flow solver. The schematic diagram of IS2 is shown in Figure 2 [11]. Position of  $\{x_{n+1/2}\}$  is predicted based on midpoint rule by using the position and velocity in displacement states vector  $\{q_n\}$  components. The position is determined by extrapolation only without integration of Eq. (8) as follows:

$$\{x_{n+1/2}\} = \{q_n\} + \frac{\Delta t}{2} \{\dot{q}_n\} \quad (14)$$

IS2 method is very similar to CS method except the extrapolation process. Therefore, the computation time of IS1 method is the same as that of CS method, but the second-order accuracy can be obtained easily. In this case, the calculated aerodynamic forces and structural position are different by half steps. The main common idea of both IS1 and IS2 is to integrate the structural Eq. (8) using the predicted aerodynamic forces by extrapolating the forces and deformation for the next step.

Finally, the main idea of the iterative staggered algorithm (ITS) suggested in this study is to repeatedly perform the explicit time integration of the structural Eq. (8) within the pseudo time loop of the flow solver to simultaneously converge the fluid solution  $\{u_{n+1}\}$  and structural position  $\{x_{n+1}\}$  in the next time step.

1. Solve the structural equation using given initial condition  $\{u_n\}$
2. Update the fluid mesh using generalized displacement vector of structural solution  $\{x^*\}$  and evaluate the  $\{u^*\}$  in fluid sub-iteration loop
3. Solve the structural equation using explicit method (RK4) with given  $\{u_n\}$  and  $\{u^*\}$  as follows:

$$\begin{aligned} \{x^*\} &= \{x_n\} + (k_1 + 2(k_2 + k_3) + k_4) / 6 \\ k_1 &= \Delta t ([A]\{x_n\} + [B]\{u_n\}) \\ k_2 &= \Delta t ([A]\{x_n + k_1 / 2\} + [B]\{(u_n + u^*) / 2\}) \\ k_3 &= \Delta t ([A]\{x_n + k_2 / 2\} + [B]\{(u_n + u^*) / 2\}) \\ k_4 &= \Delta t ([A]\{x_n + k_3\} + [B]\{u^*\}) \end{aligned} \quad (15)$$

4. If both flow and structure solutions are converged, set  $\{u^*\}$  to  $\{u_n\}$ , otherwise repeat step 2.

The solution of the structural equation usually converges more quickly than that of the flow solver in the pseudo time loop. Therefore, the efficiency of computation can be increased by introducing arbitrary variables that determine the number of couplings in the pseudo time loop of the flow solver and adjusting the information exchange period between the flow solver and the structural solver. Flowchart of a method of adjusting the coupling period by introducing an arbitrary periodic variable  $i$  is shown in Figure 3.

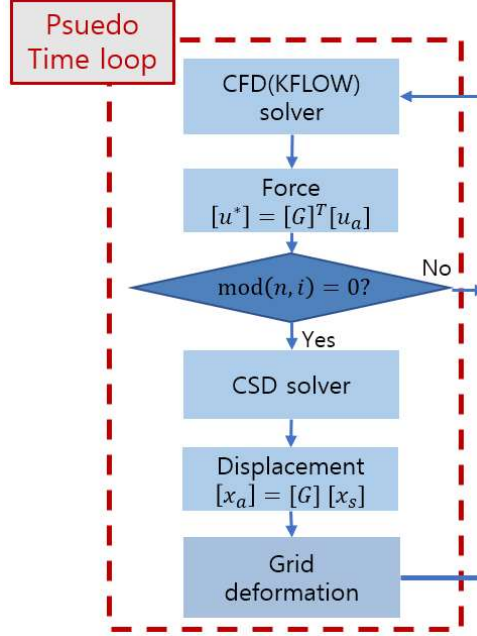


Figure 3: Flowchart of the iterative algorithm in pseudo time loop

## 2.5 Fluid-Structure Interpolating Algorithm

The thin plate spline (TPS) method used in this study provides a mean to characterize an irregular surface by using functions which minimize energy functional. The equilibrium equations between the FEM grids points and the CFD grids points are constructed by interpolation matrix for interpolating displacement vectors or projecting aerodynamic forces [12]. The number of structural nodes  $M$  and the number of nodes at the moving boundary in flow solver is  $N$ , the size of the interpolation matrix is  $M$  by  $N$ . Matrix operation takes a lot of computation time and memory. It is possible to reduce the size of the interpolation matrix by parallelizing the moving boundary of CFD grid having a relatively large size. The displacement vector obtained from the FEM grid is parallelized and interpolated to the moving boundary of CFD grid as follows.

$$\{x_f\}_K = [G]_K \{x_s\} \quad (16)$$

where  $x_f$  is the displacement vector on the divided domain of the moving boundary. The number of nodes of moving boundary is divided into  $K$  number of parallel CPUs, and the size of the interpolation matrix is  $M$  by  $N_K$ . By applying the relation between the aerodynamic forces  $\{u_f\}_K$  obtained from the divided domain and the equivalent load  $\{u_s\}$  acting on the structural grid, it can be expressed as follows.

$$\{\delta x_f\}_K^T \{u_f\}_K = \{\delta x_s\}^T \{u_s\} \quad (17)$$

Substituting Eq. (17) into Eq. (16),

$$\{\delta x_s\}^T \left( [G]_K^T \{u_f\}_K - \{u_s\} \right) = 0 \quad (18)$$

In order to satisfy the virtual displacement in Eq. (18), the following condition must be satisfied.

$$\{u_s\} = [G]_K^T \{u_f\}_K \quad (19)$$

Since the equilibrium equation is linear, it is possible to obtain the aerodynamic forces at the complete structural nodes by integrating the aerodynamic forces at each divided moving boundary.

$$\{u_s\} = \sum_{n=1}^k [G]_K^T \{u_f\}_K \quad (20)$$

### 3 Numerical Results and Discussion

#### 3.1 AGARD 445.6 wing

The AGARD 445.6 Wing was tested in the NASA Langley Transonic Dynamics Tunnel(TDT) in 1961. Flutter boundary data have been publicly available for over 20 years and have been widely used for preliminary computational aeroelastic benchmarking. Figure 4 shows the geometric configuration of AGARD 445.6 wing. The wing is a semi-span model that has the swept back angle of 45 deg along the 1/4 chord line and taper ratio 0.66. The wing cross section is symmetric NACA65A004 airfoil with a 4% thickness.

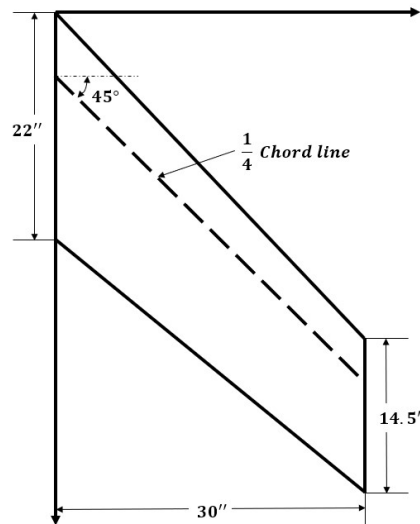


Figure 4: Geometric configuration of AGARD 445.6 wing.

First four mode shapes of the wing are shown in Figure 5. In the figure, the first and second modes are the first bending and torsion mode shapes and the third and fourth modes are the second bending and torsion mode shapes, respectively. Left figures are the FEM analysis result used in this study and right figures are the mode information presented by Yates [14]. In most of the references, four modes are used for flutter analysis. It is found that there is no significant difference in the analysis results if more modes are considered.

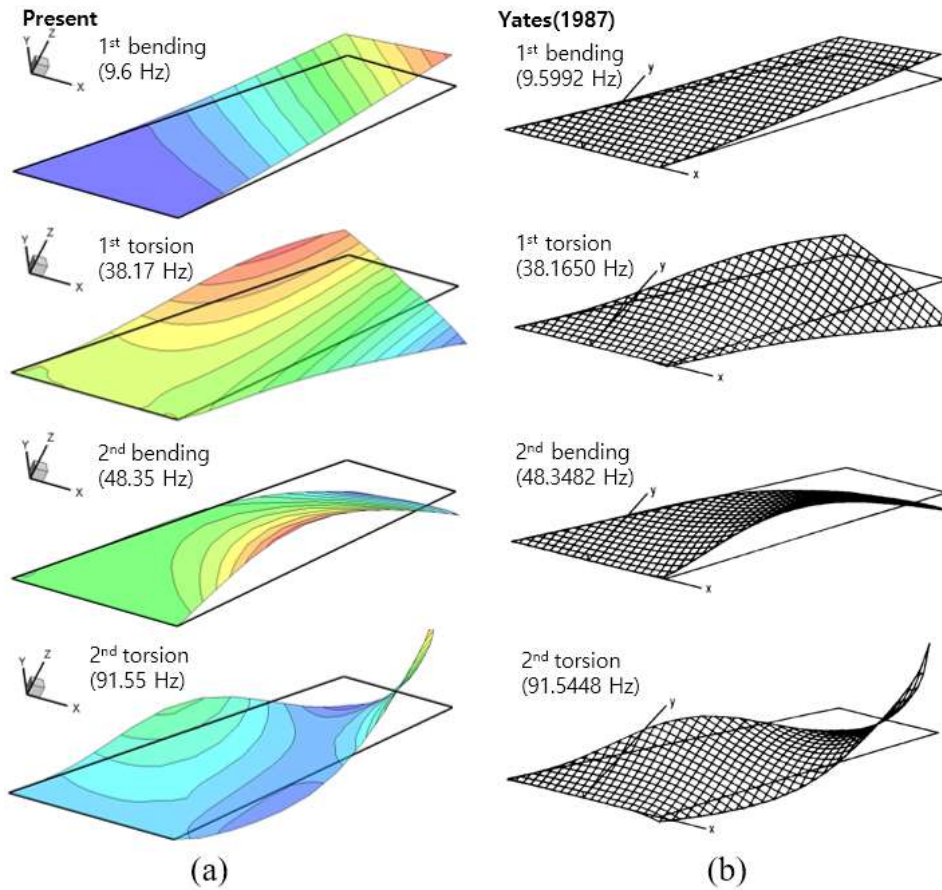


Figure 5: Structural mode shapes and frequencies.

### 3.2 Grid and Boundary Condition

Figure 6 shows the grid system used in this study. The number of grids which is the C-type topology for Euler analysis is  $144 \times 33 \times 41$  in each stream-wise, span-wise and chord-wise direction respectively. In addition, N-S base grid of  $209 \times 41 \times 65$  and N-S fine grid of  $281 \times 65 \times 97$  were used considering viscous effects using Navier-Stokes equations. Farfield boundaries of all grid systems are located 20 times the length of the chord from the wing. The surface of the wing has the adiabatic wall condition. In the case of the flutter analysis, it is difficult to consider the exact Reynolds number because the flutter speed or density is changed for each case. Applied Reynolds number on flutter boundary at  $M = 0.964$  is  $Re_c = 0.87 \times 10^6$  [22].

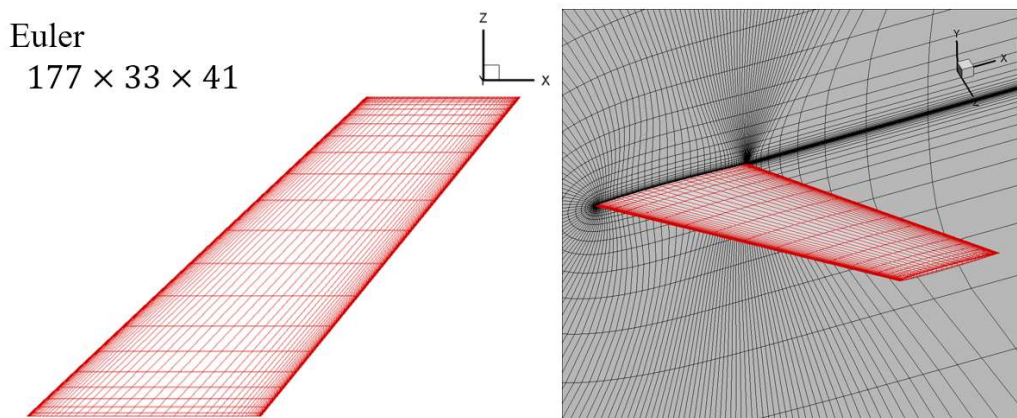


Figure 6: Structure grid system for Euler analysis

### 3.3 Code Validation using Prediction of Flutter Boundary

To verify the developed code, the Euler method and the Navier-Stokes method were used to predict the flutter boundary by varying dynamic pressure for various Mach numbers ranging from subsonic to low supersonic. The dynamic pressure at the flutter boundary is defined as flutter speed index (FSI) as follows.

$$V_f = \left( \frac{U_f}{b\omega_\alpha \sqrt{\mu}} \right)_{neutral} \quad (21)$$

$U_f$  is the free-stream velocity,  $b$  is the half root chord,  $\omega_\alpha$  is the primary torsional frequency (2<sup>nd</sup> mode) and  $\mu = m / (\rho v)$  is the wing mass ratio.  $m$  is the mass of the wing,  $v$  is the volume related to the wing, and  $\rho$  is the density of the fluid. In this study, the velocity was specified and the density was changed to check the response characteristics at the dynamic pressure corresponding to Mach number. Figure 7 shows decaying and diverging modal responses for various FSI at  $M = 0.499$ . As a result, trial and error calculations were repeatedly conducted until the neutral variations were obtained at each Mach number. Figure 8 shows the response of generalized displacements at neutral boundary for various Mach numbers.

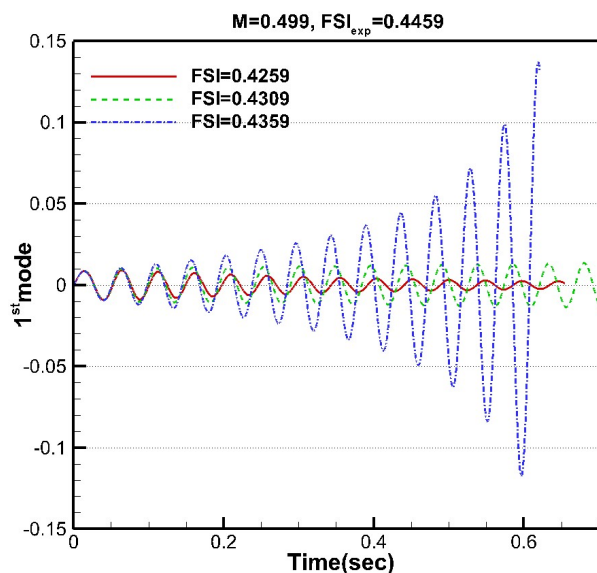


Figure 7: Decaying and diverging modal responses for various FSI (Euler,  $M = 0.499$ )

The non-dimensional time step used in all cases is set to 0.02, which means that the actual time step varies with varying flutter speeds that is equivalent to about 1/500 of the maximum period corresponding to second natural frequency. Flutter frequency ratio is  $\omega / \omega_\alpha$ ,  $\omega$  is the frequency of response of first modal displacements. Figure 9 is the flutter speed and frequency boundaries of AGARD 445.6 wing using Euler and Navier-stokes. and these results are compared with other researchers' results [6, 10, 23] and with experimental data [14]. In subsonic and transonic regions, the flutter speed was predicted to be almost equal to the experiment and well simulated flutter dip. In the low supersonic region, it has a tendency similar to other researchers' results and predicts a higher flutter speed than the experimental data. Im et al. [5] noted that it is important to accurately predict the shockwave/boundary layer interaction of the vibrating wing in the supersonic region to reduce the deviation. Accurate flutter boundary almost same as the experiment was predicted when DDES turbulence model and high order spatial discretization method are applied. The flutter boundary more slightly similar to the experimental data was predicted by using finer grid and Navier-Stokes equations.

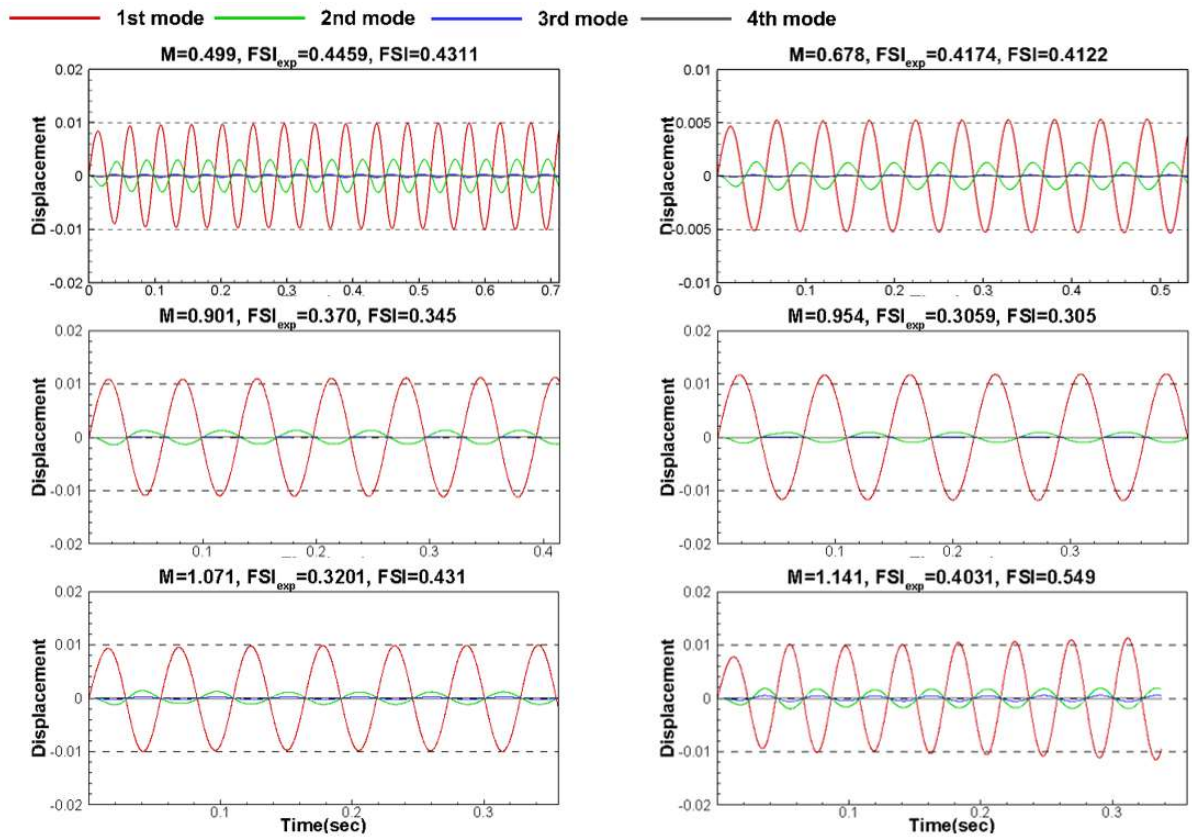


Figure 8: Generalized displacements at neutral boundaries (Euler).

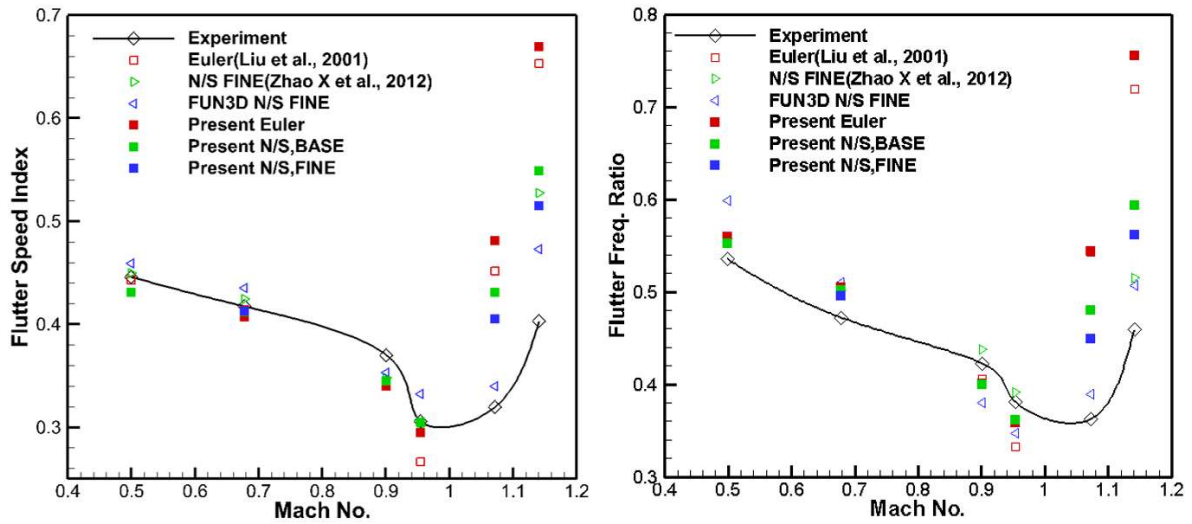


Figure 9: Flutter speed and frequency boundaries of AGARD 445.6 wing and comparisons with other researchers' results

### 3.3 Time Step Convergence

Time step convergence according to temporal scheme was investigated for the target cases with neutrally stable response at Mach numbers of 0.499 and 0.954, and the corresponding FSI was 0.4311 and 0.305, respectively. In the case of  $M = 0.499$ , the non-dimensional time step was varied from 0.0025 to 0.1. Table 1 shows the relative computation time corresponding to the non-dimensional time step used in the CFD.

Table 2: RCT according to non-dimensional time step( $M = 0.499$ )

$\Delta t^*$	RCT(ITS)	RCT(other)
0.0025	1.00	0.87
0.0050	0.68	0.59
0.0125	0.48	0.42
0.0250	0.36	0.32
0.1000	0.21	0.19

The relative computation time (RCT) is a non-dimensional computation time based on the case of ITS with the largest computation time. The computation times of the CS, IS1 and IS2 are similar while those of the ITS are increased about 15% due to the additional computations that is caused from the recurring integration of the structural dynamics and fluid dynamics. Flow solutions were converged at every time step within the L2-norm tolerance of 0.01 which is computed based on the density.

Figures 10(a) and 10(b) show the first mode response calculated by CS and ITS method, respectively. In the case of CS method, the neutral response can be obtained only when the time step size is less than 0.005. In other words, when the more smaller time step is used, the response will be more stable and convergent. In the case of ITS method, because the results do not have difference between the response which is computed with less than the 0.025 time step, all the results can be regarded as the neutral stable. we can conclude that numerical stability of the CS method is more restrictive than those of other methods, or other methods may have higher accuracy properties.

The vibration stability of the wing can be evaluated using the logarithmic decrement ratio(LDR). The definition of the LDR is as below.

$$LDR = \ln \frac{A_{i+1}}{A_i} \quad (22)$$

As the time step becomes smaller, the responses of all schemes gradually become neutrally stable, and the larger the time step, the more unstable response produces. As a result, the result with neutral response regarded as the exact solution. As the LDR approaches zero, it means that the response is more neutrally stable, and the solution is more accurate. Therefore, the accuracy can be estimated through the slope of the LDR line according to the time step, and the smaller the slope, the higher the accuracy is estimated. Figures 11 and 13 show that IS1, IS2 and ITS have almost similar accuracy but these are slightly improved in order.

Figures 12(a) and 12(b) show the first mode responses calculated by CS and ITS methods, respectively as in figures 10(a) and 10(b). The response of the CS method calculated using the largest time step of 0.8 is a very unstable response that diverges rapidly in five periods. It is considered that the temporal error has increased rapidly in a relatively large time step. ITS method converges to the neutral response for all time steps, and the response at the largest time step is indistinguishable from that predicted by the smallest time step.

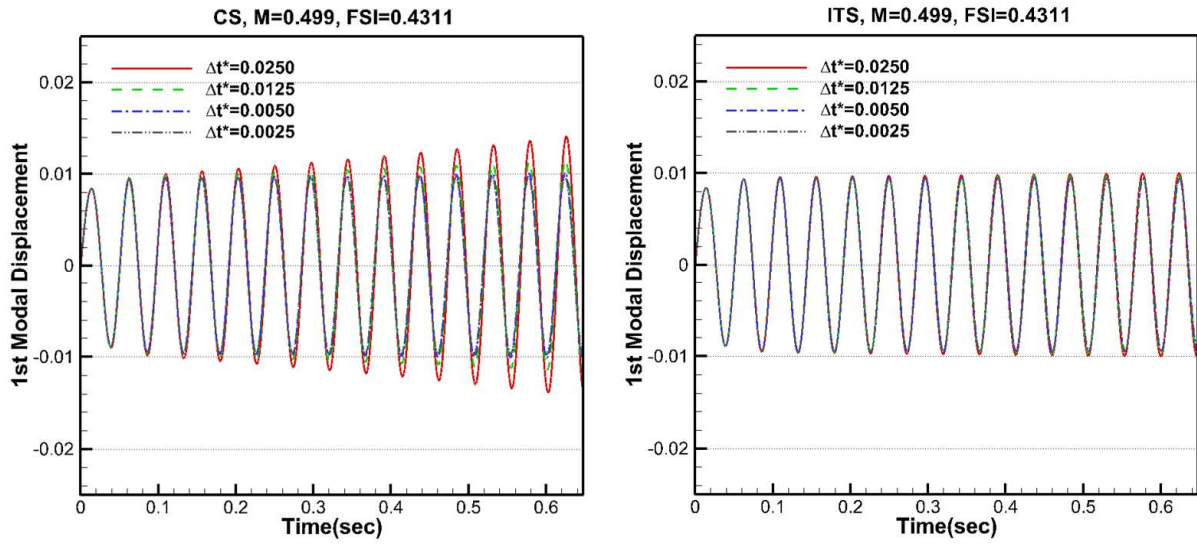


Figure 10: Time history of the first mode for various time step,  $M = 0.499$  (a: CS, b: ITS).

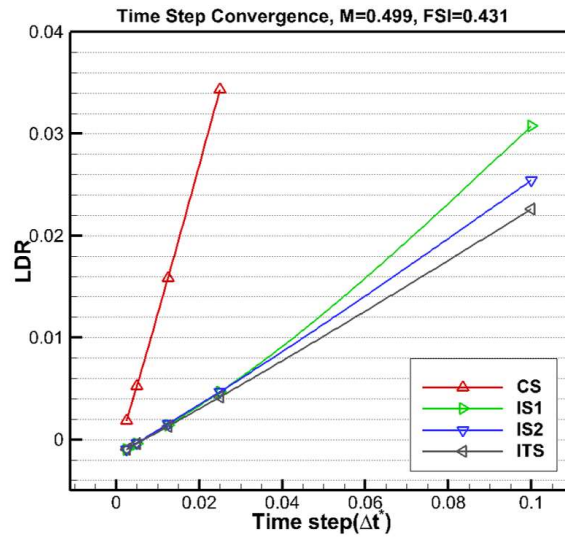


Figure 11: Logarithmic Decrement Ratio,  $M = 0.499$

Table 2: RCT according to non-dimensional time step( $M = 0.954$ )

$\Delta t^*$	RCT(ITS)	RCT(other)
0.1	1.00	0.72
0.2	0.50	0.37
0.4	0.45	0.30
0.8	0.41	0.27
1.6	0.33	0.24

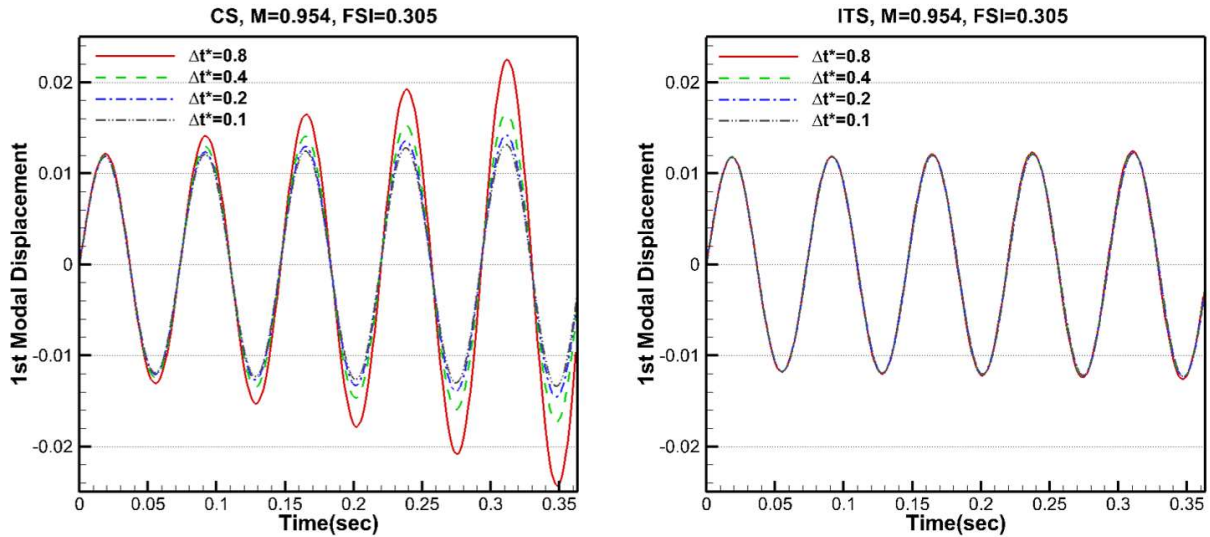


Figure 12: Time history of the first mode for various time step,  $M = 0.954$  (a: CS, b: ITS).

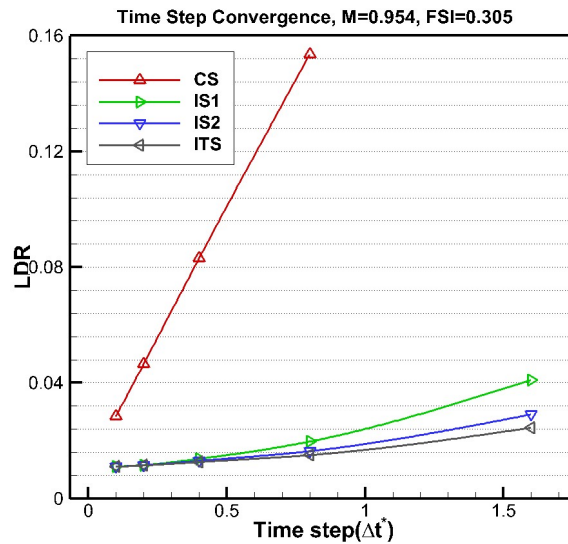


Figure 13: Logarithmic Decrement Ratio,  $M = 0.954$

## 4 Concluding Remarks

In this present study, the aeroelastic analysis system was developed by coupling between the structural dynamics based on the modal approach and an in-house CFD solver. The coupling error due to data extrapolation was reduced by the present recurring computation of the structural equation exploiting aerodynamic forces at the next time step that are computed in the pseudo time loop. The aeroelastic analysis of the AGARD 445.6 wing was conducted by the developed aeroelastic analysis system and the present results show good agreement with the experimental data. Improved staggered methods have better convergence than CS method since the structural equation was computed using fluid solution of next time step. The time step convergence test show that convergence of the ITS method is slightly improved, although the total computation time increases about 15% in the ITS method due to the additional recurring computations.

## References

- [1] H. J. Cunningham, J. T. Batina and R. M. Bennett. Modern Wing Flutter Analysis by Computational Fluid Dynamics Methods. Journal of Aircraft, Vol. 25, no. 10, pp. 962-968, 1988.

- [2] E. Lee-Rausch and J. T. Batina. Wing Flutter Computations using an Aerodynamic Model based on the Navier-Stokes Equations. *Journal of Aircraft*, Vol. 33, no. 6, pp. 1139-1147, 1996.
- [3] R. E. Gordnier and R. B. Melville. Transonic Flutter Simulations using an Implicit Aeroelastic Solver. *Journal of Aircraft*, Vol. 37, no. 5, pp. 872-879, 2000.
- [4] M. Sadeghi, S. Yang, F. Liu and H. Tsai. Parallel Computation of Wing Flutter with a Coupled Navier-Stokes/CFD method. 41st Aerospace Sciences Meeting and Exhibit, p. 1347, 2003.
- [5] H. Im, X. Chen and G. Zha. Prediction of a Supersonic Wing Flutter Boundary using a High Fidelity Detached Eddy Simulation. 50th AIAA Aerospace Sciences Meeting including the New Horizons Forum and Aerospace Exposition, p. 39, 2012.
- [6] W. A. Silva, P. Chwalowski and B. Perry III. Evaluation of Linear, Inviscid, Viscous, and Reduced-Order Modelling Aeroelastic Solutions of the AGARD 445.6 Wing using Root Locus Analysis. *International Journal of Computational Fluid Dynamics*, Vol. 28, no. 3-4, pp. 122-139, 2014.
- [7] R. Kamakoti and W. Shyy. Fluid-Structure Interaction for Aeroelastic Applications. *Progress in Aerospace Sciences*, Vol. 40, no. 8, pp. 535-558, 2004.
- [8] M. Gluck, M. Breuer, F. Durst, A. Halfmann and E. Rank. Computation of Fluid-Structure Interaction on Lightweight Structures. *Journal of Wind Engineering and Industrial Aerodynamics*, Vol. 89, no. 14-15, pp. 1351-1368, 2001.
- [9] J. Alonso and A. Jameson. Fully-Implicit Time-Marching Aeroelastic Solutions. 32nd Aerospace Sciences Meeting and Exhibit, p. 56, 1994.
- [10] F. Liu, J. Cai, Y. Zhu, A. Wong and H. Tsai. Calculation of Wing Flutter by a Coupled CFD-CSD Method. 38th Aerospace Sciences Meeting and Exhibit, p. 907, 2000.
- [11] C. Farhat and M. Lesoinne. Two Efficient Staggered Algorithms for the Serial and Parallel Solution of Three-Dimensional Nonlinear Transient Aeroelastic Problems. *Computer Methods in Applied Mechanics and Engineering*, Vol. 182, no. 3-4, pp. 499-515, 2000.
- [12] M. J. Smith, D. H. Hodges and C. E. Cesnik. Evaluation of Computational Algorithms Suitable for Fluid-Structure Interactions. *Journal of Aircraft*, Vol. 37, no. 2, pp. 282-294, 2000.
- [13] M. H. Hounjet and J. J. Meijer. Evaluation of Elastomechanical and Aerodynamic Data Transfer Methods for Non-planar Configurations in Computational Aeroelastic Analysis. National Aerospace Laboratory NLR, 1995.
- [14] E. C. Yates Jr. AGARD Standard Aeroelastic Configurations for Dynamic Response, Candidate Configuration I.-wing 445.6. 1987.
- [15] S. H. Park. Prediction Methods of Dynamic Stability Derivative Using the Navier-Stokes Equations. Doctoral Dissertation, KAIST, South Korea, 2003.
- [16] A. Jameson. Solution of the Euler Equations for Two-Dimensional Transonic Flow by a Multigrid Method. *Applied Mathematics and Computation*, Vol. 13, no. 3-4, pp. 327-355, 1983.
- [17] T. H. Pulliam. A Diagonal Form of an Implicit Approximate-Factorization Algorithm. *Journal of Computational Physics*, Vol. 39, No. 2, pp. 347-363, 1981.
- [18] H. J. Kwon. Flutter Stability Prediction using the Unsteady Aerodynamic Reduced-Order Model. Doctoral Dissertation, KAIST, South Korea, 2003.
- [19] Y. Ma, E. He, X. Zeng and J. Li. Wing Aeroelasticity Analysis based on an Integral Boundary-Layer Method Coupled with Euler Solver. *Chinese Journal of Aeronautics*, Vol. 29, no. 5, pp. 1262-1272, 2016.
- [20] N. H. Lee. Aeroelastic Analysis of Flapping Wing Using Modified Implicit Coupling Method. Doctoral Dissertation, Inha Univ., South Korea, 2017.
- [21] R. L. Harder and R. N. Desmarais. Interpolation Using Surface Splines. *Journal of Aircraft*, Vol. 9, no. 2, pp. 189-191, 1972.
- [22] L. Elizabeth M and B. John T. Calculation of AGARD Wing 445.6 Flutter Using Navier-Stokes Aerodynamics. AIAA 11th Applied Aerodynamics Conference, 1993.
- [23] X. Zhao, Y. Zhu and S. Zhang. Transonic Wing Flutter Predictions by a Loosely-Coupled Method. *Computers & Fluids*, Vol. 58, pp. 45-62, 2012.